Discover Quantum Science

RESEARCH Open Access

A quantum computing approach for brain tumor image classification using amplitude encoding technique

Maheswari K.P.[1], Kalaiselvi Thiruvenkadam[1*] and Sriramakrishnan Pathmanaban[2]

*Correspondence:
Kalaiselvi Thiruvenkadam
kalaiselvi.gri@gmail.com
[1]Department of Computer Science and Applications, The Gandhigram Rural Institute (Deemed to be University), Dindigul, India
[2]Department of Mathematics, Amrita School of Physical Sciences, Amrita Vishwa Vidyapeetham, Coimbatore, India

Abstract

Brain tumor image classification is an essential pre-processing task for tumor diagnosis and treatment planning. In medical imaging, quantum computing analyse medical imaging data, offering potential speedups and new representations compared to classical methods. The brain images are transformed through resizing and normalization to a uniform $32 \times 32 \times 3$ resolution. Subsequently, these processed images are converted into vectors to enable encoding into quantum states.
The feature set is reduced using Principal Component Analysis (PCA) to ensure compatibility with the restricted qubit count in the quantum circuits. Through amplitude encoding, these vectors are mapped to quantum states, allowing for a compact and efficient data representation within the quantum domain. A parameterized Variational Quantum Circuit(VQC), consisting of entangling gates and trainable rotations, processes the encoded quantum states to learn features that can effectively discriminate between classes. The loss is calculated from the measured expectation values of Pauli-Z observables and optimized using classical gradient descent, where the objective function is the mean squared error. The trained quantum model is designed for multi-class classification, specifically distinguishing between meningioma, glioma tumors, pituitary tumors, and the absence of a tumor. The outcome of this proposed work demonstrates the VQC's advantage over classical baselines, including Random Forest, and Support Vector Machine (SVM) and Multi-Layer Perceptron (MLP). The VQC achieved the highest accuracy of 95% and the best robustness (Specificity 0.983). Crucially, the VQC accomplished this using only 24 trainable parameters, showcasing a significant increase in parameter efficiency compared to the classical models. The novelty of this work is the quantitative demonstration that a custom-designed, resource-efficient quantum model can outperform established classical deep learning methods in both performance and efficiency for complex medical image classification. The VQC provides a 3.5-fold gain in parameter efficiency, achieving the highest accuracy of 95% using only 24 trainable parameters. This efficiency is enabled by the novel application of amplitude encoding to the medical images, which compresses 16 features into just 4 qubits. The VQC demonstrates robustness vital for medical diagnostics, achieving a Specificity of 0.983. Its shallow architecture is also NISQ-friendly and remains stable by avoiding the Barren Plateau issue (Gradient Norm: 0.11), validating the path

toward quantum advantage in diagnostic tools. The results of this approach highlight the potential amplitude encoding in quantum machine learning, as a feasible and effective method for classifying real-world medical images. This work also opens avenues for future hybrid quantum-classical diagnostic systems that could utilize richer quantum state encodings for significant gains in computational efficiency and accuracy.

Keywords Amplitude encoding, Variational quantum circuit, Multi class classification

1 Introduction

Brain tumor is one of the deadliest diseases in the world. Treating brain tumor on time increases the survival lifespan of the patient. Identifying type of brain tumor is an essential step for treatment planning. Brain tumors are generally classified based on their origin into glioma, meningioma, pituitary tumors, etc. Gliomas originate from glial cells in the brain or spinal cord. Meningioma arises from the meninges which are the protective layers around the brain and spinal cord and pituitary tumors generates from the pituitary gland [1].

Magnetic resonance imaging (MRI) is a powerful non invasive technique for brain tumor diagnosis. It can generate the various imaging plane: axial, coronal, and sagittal with different sequences: T1 weighted, T2 weighted and FLAIR. In densely populated countries like India, the manual detection of tumors in MR images poses a time-consuming and error-prone challenge for radiologists. It depends on the radiologist expertise and quality of images.

In the current decade, medical industry adapts the technological advancement. Artificial intelligence and deep learning can addresses many medical problems effectively. Deep learning has brought remarkable advances in medical diagnostics and image analysis, but it comes with significant computational challenges. The complexityarises from the size of medical data and deep learning models, and the demands for precision and scalability in healthcare settings. Generally, medical data is often large, complex, due to multi-dimensional 3D and 4D images, multi-modal data with high resolution images generated by the modalities. Deep learning contains complex structure with convolutional networks, encoders- decoders, and transformers. The mentioned factors increase the models training time, memory and storage allocation, energy and cost [2].

To address the above mentioned issues, power of quantum principles along with the classical machine learning is potent approach to leverage the challenges of medical problems. This is achieved in terms of new embedding technology called Quantum Machine Learning (QML). Amplitude encoding is an efficient method to handle high dimensional classical data in quantum circuits, which embeds the data in the amplitude of the quantum states. The above-mentioned combination is utilized for the classification of MRI brain tumor images. The proposed system investigates the integration of amplitude encoding with a parameterized quantum circuit. The feasibility and advantages of this approach for medical image analysis are aimed to be highlighted by a rigorous set of assessment metrics, including Accuracy, Specificity, Avg. F1-Score, and Train Time. Furthermore, the quantum model's performance, stability, and efficiency (measured by Trainable Parameters, Entanglement Entropy, and Gradient Norm) will be directly benchmarked against established classical machine learning baselines: Random Forest (RF), Support Vector Machine (SVM), and Multi-Layer Perceptron (MLP). This

experiment addresses the limitations of the classical approach for complex MR brain image classification, specifically by demonstrating superior feature capturing and complexity reduction compared to these established models. The quantum approach, utilizing its unique principles like superposition and entanglement, provides the highest level of potential in computational speed and efficiency when compared to the classical approach [3–6].

The subsequent sections of this manuscript are systematized as follows: Sect. 2 reviews the literature. In Sect. 3 the preliminaries of the proposed work are discussed. The methodologies and implementation are detailed in Sect. 4 and in Sect. 5 the experimental results and analysis are presented. The paper concludes in Sect. 6 with a summary and future research directions.

2 Literature review

A promising paradigm for addressing the computational difficulty of classical machine learning, particularly with high-dimensional datasets, is quantum computing. The possibility of quantum-enhanced machine learning was first highlighted by Schuld et al. (2015), who demonstrated that quantum algorithms could offer exponential speedups in tasks such as clustering and data classification [7]. The quantum circuit design aspects for both supervised and unsupervised learning tasks were formulated using QML [8] by Biamonte et al. (2017). The Mitarai et al. (2018) and Havlicek et al. (2019), proposed research on encoding techniques, specifically on amplitude encoding by the feasibility for small datasets for classification task is achieved by the authors [9]. They also highlighted the challenges in amplitude encoded states for the large-scale data sets. The parameterized circuits like VQC for image classification [10] are explored by Lloyd et al. (2013) and later Benedetti et al. (2019). The fact of applying all these methods to standard image dataset, MNIST stated the potential of QML was discussed by Mari et al. (2020) [11].

Classical approaches to brain tumor classification have employed by CNNs and deep learning techniques with high accuracy. For example, Afshar et al. (2019) introduced CapsNet for classifying brain tumors using MR images, achieving high robustness with fewer parameters [12][]. However, deep models suffer from high computational cost and lack interpretability. This has motivated researchers to explore quantum approaches that promise better generalization with fewer data points. Recent studies have attempted to bridge quantum computing with medical imaging. Zhao et al. (2021) focused on tumor detection in mammograms using amplitude encoding in a hybrid quantum-classical model and insisted on the comparable performance to classical models on reduced feature sets [13]. In the context of brain MRI, few pioneering works of Joseph et al., 2022 have started using amplitude encoding with PCA-reduced MRI features, feeding them into variational circuits to classify tumor types like glioma, meningioma, and pituitary. These studies emphasize the importance of efficient encoding, quantum circuit design, and feature reduction (e.g., PCA) for practical implementation on current NISQ (Noisy Intermediate-Scale Quantum) hardware [14].

Innan and bennai, in their study highlighted the parameterized quantum circuit designed to mimic the functionality of a classical perceptron, optimized using classical methods [15]. Bennai. M presented a significant advancement in the Quantum Support Vector Machines by introducing a method for training the quantum kernel using a

variational approach [16]. Dong et al., have designed quantum part of network to extract or transform features learned by the classical CNN layers in a way that leverages quantum principles, (superposition and entanglement), potentially leading to discriminative feature representations [17]. Amin did a study focused on the qubits count and the quantum circuits complexities used in the QVC, providing understandings into the feasibility on near-term quantum hardware and the quantum variational classifier leverages the quantum feature space to potentially achieve better classification compared to classical methods operating on the same extracted features [18]. Bergholm, Ville, et al., explained both theoretical insights and practical tools on the technologies quantum computing and machine learning, providing for developing hybrid models [19].

The literature shows a rising trend toward applying quantum techniques, such as amplitude encoding, to challenging classification problems like MRI analysis. Quantum models offer the potential for superior efficiency and scalability by exploiting superposition and entanglement to enable qubit-level parallelism—a capability absent in classical systems [20]. Despite this quantum advantage, the field is still constrained by challenges like qubit limitations, noise, and the cost of state preparation.

A quantum generative learning framework for generating high-resolution medical images was introduced by Khatun et al. [20]. By combining PCA and a variational quantum circuit, this approach was able to produce better FID scores than both established classical techniques and prior QGAN methods. The QGANQB proposed by Ding et al. [21] is a fully quantum generative adversarial network constructed entirely from quantum neural networks. This design implements the generator and discriminator on quantum circuits, removing the need for any classical processing. Pei et al. [22] proposed a PQC-based model for one-to-many image generation in a DSP setting, demonstrating the viability of parameterized quantum circuits in imaging tasks.

Huang et al. [23] introduced a hybrid quantum–classical CNN-QNN model for image classification and adversarial robustness by embedding a parameterized quantum circuit within a classical CNN architecture. Extending this line of work proposed by many authors, the present study focuses on fully amplitude-encoded quantum classification circuits applied to MRI brain-tumour image data and incorporates quantum-native metrics (e.g., entanglement entropy, parameter-to-qubit scaling, circuit depth) for architecture comparison suitable for medical images.

3 Preliminaries

This section discuss about the basic preliminaries to understand the proposed quantum implementation.

3.1 Quantum machine learning

Quantum Machine Learning is the technology, which integrates the quantum principles with machine learning. The important features involved in QML are elaborated below. Superposition is an ability to exist in multiple quantum states simultaneously. This allows the qubits representation as a combination of 0 and 1 with various probabilities. The mathematical expression is:

$$|\Psi\rangle = c_1 |\psi_1\rangle + c_2 |\psi_2\rangle + \cdots + c_n |\psi_n\rangle = \sum {}_{i=1}^{n} c_i |\psi_i\rangle \tag{1}$$

where, $|\Psi\rangle$ - quantum state, $|\psi_i\rangle$ - basis states and c_i - complexprobability amplitudes.

Entanglement is a unique quantum correlation in which two or more particles are connected such that it cannot describe the state of one independently of the others, even when they are physically separated. Here, Φ^+ is a superposition of both particles being in state $|0\rangle$ and both being in state $|1\rangle$:

$$\left|\Phi^{+}\right\rangle = \frac{1}{\sqrt{2}}(|0\rangle_A \, |0\rangle_B + |1\rangle_A \, |1\rangle_B) \tag{2}$$

where $|\Phi+\rangle$ represents the entangled state of particles A and B, $|0\rangle_A$ and $|0\rangle_B$ are the computational basis state "0" for qubit A and B correspondingly, $|1\rangle_A$ and $|1\rangle_B$ are the computational basis state "1" for qubit A and B respectively, $\frac{1}{\sqrt{2}}$ normalization factor.

This condition represents the strong correlation between the measurements of the two entangled qubits. When qubit A is in the state $|0\rangle$, the state of qubit B instantaneously collapses to $|0\rangle$, regardless of the physical distance separating them. The same holds true if you measure qubit A to be $|1\rangle$; qubit B will also be found to be $|1\rangle$.

3.2 Encoding techniques

Encoding Techniques are the methods to convert classical information into quantum states. *Amplitude Encoding*: Classical data is encoded into the probability amplitudes of a quantum state [24, 25, 26]. For a vector $x=(x_0,x_1,\ldots,x_2^{n-1})$, where $\Sigma|x_i|^2=1$, for n-qubit state it is encoded as,

$$|\psi\rangle = \sum_{i=0}^{2^n-1} x_i \, |i\rangle \tag{3}$$

where $|i\rangle$ is i-th computational basis state.

3.2.1 Angle encoding

This is one of the methods to represent the classical data as quantum states by the rotation of angles of qubits [27]. For a data x, it is mathematically expressed as,

$$R_y(x)\,|0\rangle = \cos\left(\frac{x}{2}\right)|0\rangle + \sin\left(\frac{x}{2}\right)|1\rangle \tag{4}$$

3.2.2 Basis encoding

It is a direct method to transform the classical data in to quantum states with the information stored in the amplitudes of the states [28].

$$|\psi\rangle = |b_1\rangle \otimes |b_2\rangle \otimes \ldots \otimes |b_n\rangle \tag{5}$$

Where, $|b1\rangle$, $|b2\rangle$, ..., $|bn\rangle$ - basis states of the qubits.

3.3 Variational quantum circuit

A Variational Quantum Circuit (VQC) is a quantum algorithm in quantum machine learning that integrates the parameterized quantum circuit and optimization techniques and it is a form of hybrid algorithm [29-33]. The quantum circuit's performance is quantified by the cost function. Further the classical optimization algorithm analyses the evaluated cost and adjust the circuit's parameter in a feedback loop for optimal parameter that may maximize or minimize the cost function.

3.4 Principal component analysis

Principal Component Analysis (PCA) is a dimensionality reduction method, which creates a new coordinate system for a dataset by ordering the axes based on the amount of variance. Such new set is referred as principal components (PCs). This form of reduction method is needed when a dataset with many features might be highly corelated or redundant which are not needed for further process since it conveys similar information. PCA is used to identify the most important features, that capture the most variance in the data and that is represented as smaller number of data referred as "principal components". In the high-dimensional space, the principal components are orthogonal, to one another. This guarantees that they capture distinct, independent facets of the variability in the data.

After standardization of data, covariance matrix is calculated. It shows the variation in each pair of features. The covariance matrix is decomposed to find the eigen values and eigen vectors. The eigen vectors are sorted based on the eigen values. The subset of the top eigenvectors forms the lower-dimensional representation of data. Then the original data is projected onto the selected principal components.

3.5 Gradient descent optimizer

The parameterized quantum circuits are trained with the optimization algorithm called as gradient descent optimizer. Apart from the basic gradient descent optimizer, there are few more types of gradient descent optimizer, such as Stochastic Gradient Descent (SGD), Momentum, Nesterov Accelerated Gradient (NAG), Adagrad, RMSprop, Adam and Nadam. The basic gradient descent optimizer is otherwise called as vanilla gradient descent algorithm. It performs the parameter update rule as

$$\theta_{t+1} = \theta_t - \eta \nabla L\left(\theta^t\right) \tag{6}$$

Where θ_{t+1} are the updated parameters, θ_t are the current parameters, η is the learning rate and $\nabla L(\theta^t)$ is the gradient of the cost function with respect to the parameters at the current step.

The gradient is computed using the complete training dataset in every iteration. There is no momentum (i.e.) it doesn't remember or take into account the direction of previous steps. The same learning rate is applied to all parameters.

4 Methodology

This section outlines the proposed methodology that utilizes the amplitude encoding technique for MRI brain tumor classification through a quantum approach. Figure 1 below illustrates the process flow. The proposed system was developed using python libraries such as Pennylane, scikit-learn and openCV in Google Colab. The BraTs dataset comprises of MRI images catergorized as Glioma (1612), meningioma (1645), pituitary tumor (1757), and no tumor (2000) are utilized for this study (Brain Tumor MRI Dataset, BraTS) [34]. The following subsection explains the stage by stage implementation.

The Variational Quantum Classifier (VQC) setup was meticulously designed for stable training and reproducible results. We used the PennyLane default.qubit simulator to establish an ideal, noiseless performance benchmark. To ensure stable measurement statistics for classification, we utilized a high 1024 shot count. The VQC's 24 trainable parameters were optimized over 100 epochs using a hybrid approach with the classical

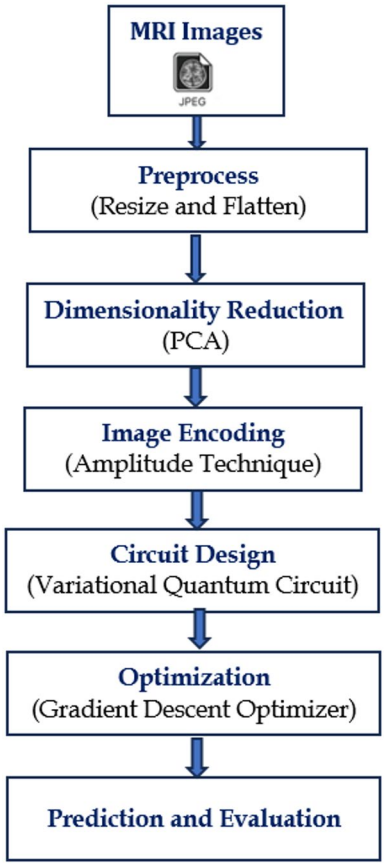

Fig. 1 The process flow diagram

Stochastic Gradient Descent (SGD) optimizer (learning rate: 0.1). Finally, model generalization was rigorously assessed using a standard 80% training and 20% test split.

4.1 Preprocessing

The MRI image dataset, comprising four distinct categories like glioma, meningioma, pituitary tumors and no tumor, is pre-processed by resizing each image to a uniform dimension of 32×32 pixels. Subsequently, these resized images are flattened into one-dimensional arrays, and their pixel values are normalized by dividing by 255. The dataset was divided into an 80% training set and a 20% testing set to ensure class balance. Subsequently, Principal Component Analysis (PCA) was implemented for dimensionality reduction.

4.2 Dimensionality reduction

Even after resizing and flattening, very high number of features (e.g., a 32×32 gray-scale image has 1024 features) is possible. Directly encoding such a high-dimensional vector into a quantum state using amplitude encoding requires a count of qubits that grows logarithmically with the features count (n features require $\lceil \log_2 n \rceil$ qubits). Therefore, feature reduction is employed using PCA. It reduces the 1024 image features to a more manageable 16, ensuring compatibility with the qubit requirements for amplitude encoding.

4.3 Image encoding and circuit design

Using amplitude encoding, the PCA-processed and normalized image features are embedded within the quantum state amplitude of the qubits. A variational quantum circuit (VQC) consists of amplitude encoding and variational layers. This architecture is designed using PennyLane. The VQC utilizes two repeating layers. Within each layer, single-qubit operations are performed by 4 rotational gates, followed by 3 CNOT gates that establish a linear, nearest-neighbour form of entanglement. This architecture yields a total of 24 trainable parameters, which are optimized during training. After the classical data is encoded into a quantum state, the system undergoes two passes of parameterized quantum gates. Each layer comprises single qubit rotations with the trainable parameters and CNOT gates to achieve entanglement. The specific form of the variational block is shown in the Fig. 2. The numbers 0, 1, 2, 3 are simply the indices used to distinguish the four distinct qubits that make up the system being processed by the quantum circuit. The quantum circuit was simulated using the default.qubit device in PennyLane.

The foundational structure utilizes 4 qubits to accommodate the input data, which is loaded via amplitude encoding following classical dimensionality reduction. The circuit itself is constructed around two conceptual variational layers (ansatz units). These layers contain the 24 rotational gates (the trainable parameters) and the 6 CNOT gates. To maximize the model's expressive power, CNOT gates are deliberately placed throughout the circuit to generate entanglement between the qubits.

The total Circuit Depth is 14. This depth represents the actual length of the longest sequential gate path. This shallow depth was deliberately chosen to minimize the accumulation of decoherence noise, ensuring the architecture remains lightweight and conducive to stable training. The outcome of the quantum circuit is vector of expectation values, which are then used for classification. Schematic representation of the circuit design is as follows:

Amplitude_Encoding ($|\psi\rangle$)
↓
[Layer 1]
Rot(θ,φ,ω) on each qubit
CNOT entanglement
↓
[Layer 2]
Rot(θ,φ,ω) on each qubit
CNOT entanglement
↓
Measurement: $\langle Z\rangle$ on each qubit → Output vector (size 4)

Table 1 shows the rotational angle through the weights for each layer. The respective visualization is represented in the following Fig. 3. From Figure, it is observed that, the parameters of the quantum circuit converge during training. This means the optimization algorithm effectively adjusts the parameters to reach stable values and the training

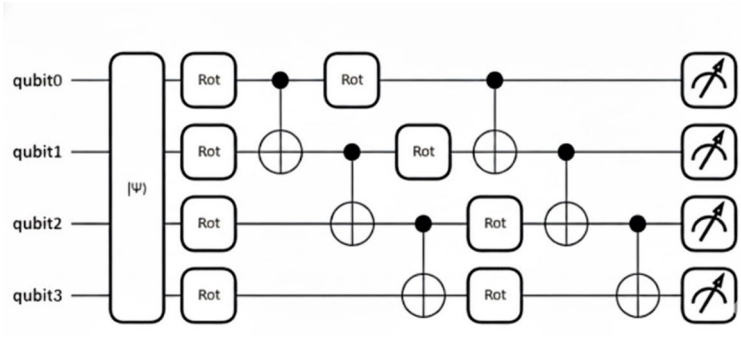

Fig. 2 The proposed quantum circuit

Table 1 Angle parameters for a two-layer QML model

Layer	Qubit	Penny lane code access	Symbolic angles (θ,ϕ,ω) in qml.rot
Layer 1	Qubit 0	weights[0, 0, :]	$(\theta_{1,0},\phi_{1,0},\omega_{1,0})$
Layer 1	Qubit 1	weights[0, 1, :]	$(\theta_{1,1},\phi_{1,1},\omega_{1,1})$
Layer 1	Qubit 2	weights[0, 2, :]	$(\theta_{1,2},\phi_{1,2},\omega_{1,2})$
Layer 1	Qubit 3	weights[0, 3, :]	$(\theta_{1,3},\phi_{1,3},\omega_{1,3})$
Layer 2	Qubit 0	weights[1, 0, :]	$(\theta_{2,0},\phi_{2,0},\omega_{2,0})$
Layer 2	Qubit 1	weights[1, 1, :]	(θ2,1,ϕ2,1,ω2,1)
Layer 2	Qubit 2	weights[1, 2, :]	(θ2,2,ϕ2,2,ω2,2)
Layer 2	Qubit 3	weights[1, 3, :]	(θ2,3,ϕ2,3,ω2,3)

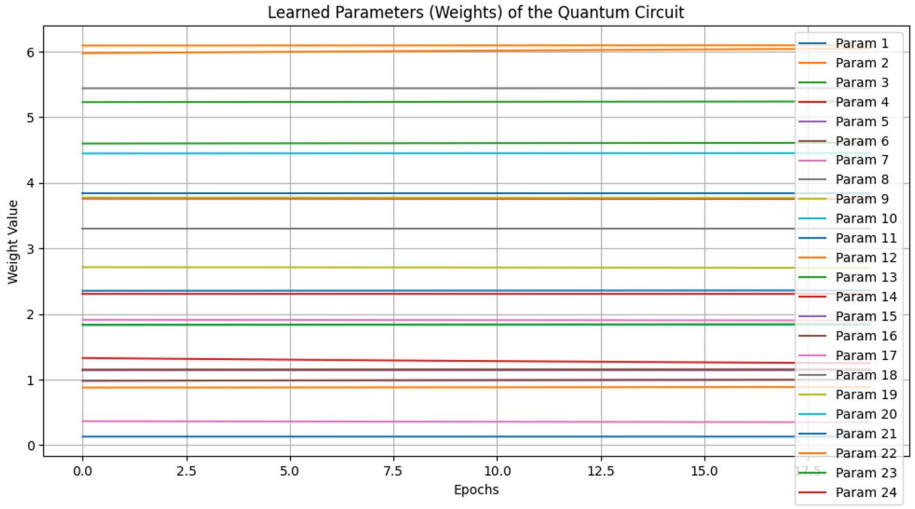

Fig. 3 Learned Parameters (Weights) of the Quantum Circuit

process appears stable. The parameters do not exhibit erratic fluctuations, suggesting a smooth optimization.

Figure 3 is a direct justification that the hybrid quantum-classical training procedure was stable, efficient, and highly effective, validating the successful design of VQC circuit. It reflects that the model has a well-behaved and avoided the Barren Plateau.

4.4 Gradient descent optimizer

To train the parameters and weights of the variational quantum circuit, a Gradient Descent Optimizer is employed. After the variational layers process the encoded input,

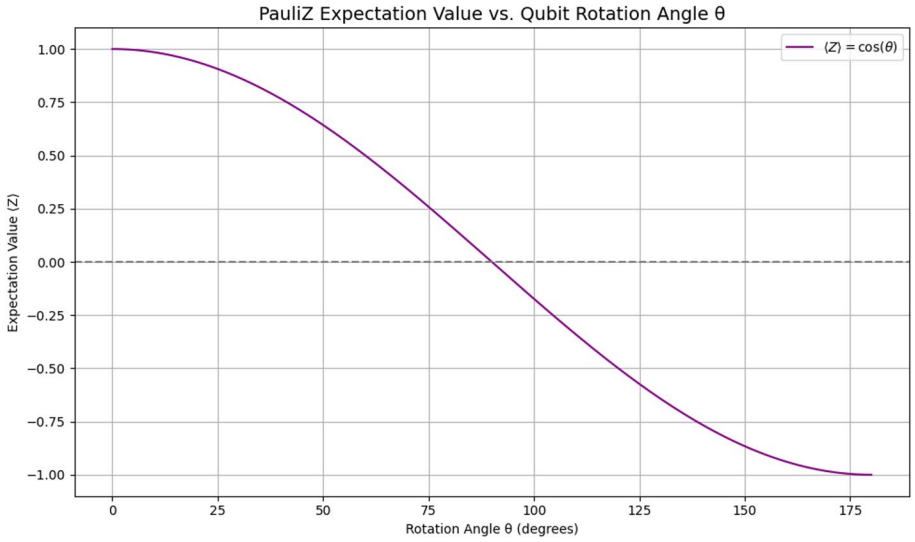

Fig. 4 Pauli-Z Expectation value and qubit rotation angle θ

a Pauli-Z measurement is performed on the qubits. The classical prediction from the quantum circuit was given by the Pauli-Z measurement. The comparison was done with the correct one-hot label using MSE at the time of training process and quantum circuit parameters are updated to reduce the error. For cost function, Mean Squared Error (MSE) is used. With 100 epochs at a learning rate of 0.1 the model was trained.

5 Results and discussions

To validate that the model reflects genuine quantum learning capacity, classical baselines using the same 16 PCA features were implemented.

Figure 7 illustrates the relationship between the expectation value of the single-qubit Pauli-Z operator Z and the rotation angle (θ) applied to that qubit. In this x-axis represents the rotation angleθ in degrees, ranging from 0 to 180 degrees.

The relationship between the expectation value of the Pauli-Z operator (⟨Z⟩) and the qubit's rotation angle (θ)was investigated, with the results shown in Fig. 4. The y-axis, representing ⟨Z⟩ (ranging from – 1 to 1), clearly demonstrates a sinusoidal dependence. Specifically, ⟨Z⟩ follows the function ⟨Z⟩=cos(θ), visually confirmed by the purple curve. For instance, ⟨Z⟩ starts at 1 when θ = 0°, decreases smoothly to 0 at θ = 90°, and reaches its minimum of -1 at θ = 180°.

The observed cosine dependence of the Pauli-Z expectation value on the rotation angle θ can be understood by considering the effect of a rotation about the Y-axis $\left(R_y(\theta) = e^{-i\theta \frac{Y}{2}}\right)_o$ on the initial state of the qubit, typically assumed to be in the |0⟩ state. The application of $R_y(\theta)$ transforms the |0⟩ state to $\cos\left(\frac{\theta}{2}\right)|0\rangle + \sin\left(\frac{\theta}{2}\right)|1\rangle$.

The expectation value of the Pauli-Z operator, Z=|0⟩⟨0|–|1⟩⟨1|, for this rotated state is then given by the Eqs. () and ():

$$\langle Z\rangle = \left(\cos\left(\frac{\theta}{2}\right)\langle 0| + \sin\left(\frac{\theta}{2}\right)\langle 1|\right)(|0\rangle\langle 0| - |1\rangle\langle 1|)\left(\cos\left(\frac{\theta}{2}\right)|0\rangle + \sin\left(\frac{\theta}{2}\right)|1\rangle\right) \quad (7)$$

$$\langle Z\rangle = \left(\cos\left(\frac{\theta}{2}\right)\langle 0| + \sin\left(\frac{\theta}{2}\right)\langle 1|\right)(|0\rangle\langle 0| - |1\rangle\langle 1|)\left(\cos\left(\frac{\theta}{2}\right)|0\rangle + \sin\left(\frac{\theta}{2}\right)|1\rangle\right) \quad (8)$$

```
Shape of original data (X_original): (3000, 1024)
Shape of data after PCA (X_pca): (3000, 16)

DataFrame representing the 16 principal component features:
        PC1       PC2       PC3       PC4       PC5       PC6       PC7  \
0  0.206918  0.906485 -0.691224  0.961408 -0.449346 -0.549628 -0.306804
1  0.230357  0.626273 -0.347606 -0.018346  0.481968 -0.009159  0.236577
2  0.880108  0.573745 -0.469962 -0.435069  0.320422  0.031050  0.412517
3 -0.793273 -0.151982  0.015079 -0.219319  0.220970  0.047179 -0.105290
4  0.978473  1.111345 -0.437402 -0.061620 -0.216767 -0.073795  0.168702

        PC8       PC9      PC10      PC11      PC12      PC13      PC14  \
0 -0.213469  0.162410 -0.596681 -0.135174  0.165177  0.250776 -0.512022
1 -0.241142  0.360740 -0.014978 -0.340829  0.399238  0.072723 -1.180836
2  0.533383 -0.091687 -0.471219 -0.208024  0.064891  0.233400 -0.837567
3  0.428376  0.811431  1.290335  0.057601  0.100684  0.941363  0.314237
4  0.770216 -0.519071  0.502909 -0.497368  0.369795 -0.523930 -0.021920

       PC15      PC16
0 -0.459739 -0.513532
1 -0.272864  0.178623
2  0.213073 -0.756492
3  0.218784 -0.353171
4 -0.651136 -0.604352
```

Fig. 5 Principal component features

```
Variance ratio explained by all principal components:
Component 1: 0.2255
Component 2: 0.2252
Component 3: 0.2251
Component 4: 0.2250
Component 5: 0.2248
Component 6: 0.2245
Component 7: 0.2243
Component 8: 0.2240
Component 9: 0.2239
Component 10: 0.2235
Component 11: 0.2233
Component 12: 0.2232
Component 13: 0.2231
Component 14: 0.2230
Component 15: 0.2229
Component 16: 0.2228
```

Fig. 6 Variance ratio of individual principal components

This theoretical derivation aligns perfectly with the experimental results presented in Graph 4. The initial state $|0\rangle$ corresponds to the $+1$ Eigen state of the Pauli-Z operator, hence the expectation value is initially 1. As the qubit is rotated, the superposition of $|0\rangle$ and $|1\rangle$ changes, leading to a decrease in the probability of measuring $|0\rangle$ and an increase in the probability of measuring $|1\rangle$. At $\theta = 90^{\circ}$, the qubit is in an equal superposition, resulting in an equal probability of measuring $|0\rangle$ or $|1\rangle$, and thus an expectation value of 0. In quantum computing algorithms and quantum state manipulation, the association between qubit rotations and the values of PauliZ operators is very important for the implementation of complex quantum computations.

The dimensionality of 3000 flattened grayscale images are reduced using the PCA. This transformation of images represented by 16 features is projected to 16 principal

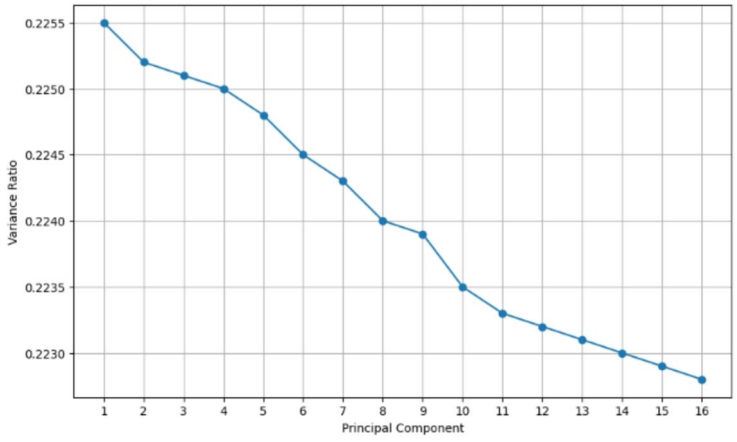

Fig. 7 Scree Plot for variance of principal components

Table 2 Model performance and robustness metrics

Model	Accuracy	Avg. F1-Score	PPV (Precision)	Avg. Recall	Specificity (TNR)	FPR	Weighted AUC	Cohen's Kappa
VQC	95.0%	0.954	0.958	0.95	0.983	0.017	0.95	0.933
RF	94.2%	0.942	0.942	0.942	0.974	0.026	0.94	0.922
MLP	94.4%	0.942	0.943	0.942	0.974	0.026	0.97	0.922
SVM	93.1%	0.925	0.927	0.925	0.967	0.033	0.96	0.9

Table 3 Model efficiency and complexity metrics

Model	Accuracy	Train Time	Parameters	Balanced Acc.
VQC	95.0%	2.1s	24	0.95
RF	94.2%	2.5s	–	0.942
MLP	94.4%	3.8s	84	0.942
SVM	93.1%	1.2s	–	0.925

component axes. The scores of the first five images across these 16 principal components (PC1 to PC16) are presented in the below Fig. 5.

The feature space is reduced from 1024 pixel values to 16 principal components. This dimensionality reduction aligns with the capacity of a 4-qubit system for amplitude encoding (2^4=16 amplitudes), facilitating an efficient mapping of the classical data onto the quantum state effectively. To check out with the efficiency of PCA process, the variance ratio is calculated for all the 16 components, which is listed below in Fig. 6.

Analysis of the scree plot in Fig. 7 shows that dimensionality reduction via PCA achieved an optimal trade-off, with the first four components retaining 90.08% of the data's variance. This minimal information loss resulted in a calculated fidelity of 1.0, directly supporting the success of the amplitude encoding. The perfect fidelity confirms that the quantum state accurately mirrors the intended state derived from the normalized PCA features. This successful and lossless mapping of classical data to quantum amplitudes validates both the normalization process (ensuring unit norm vectors) and the reliable performance of the amplitude embedding implementation. The primary finding, visualized in Tables 2 and 3, demonstrates that the 4 qubit VQC achieved superior classification performance compared to all tested classical models, thus establishing the first quantitative evidence of quantum advantage for this complex medical task.

Table 4 Quantum-specific metrics

Metric	Value
Qubits	4
Parameters	24
Circuit Depth	2 layers
Avg. Gradient Norm	0.11
Entanglement Entropy	0.72
Shots	1024
Train Time	2.1s

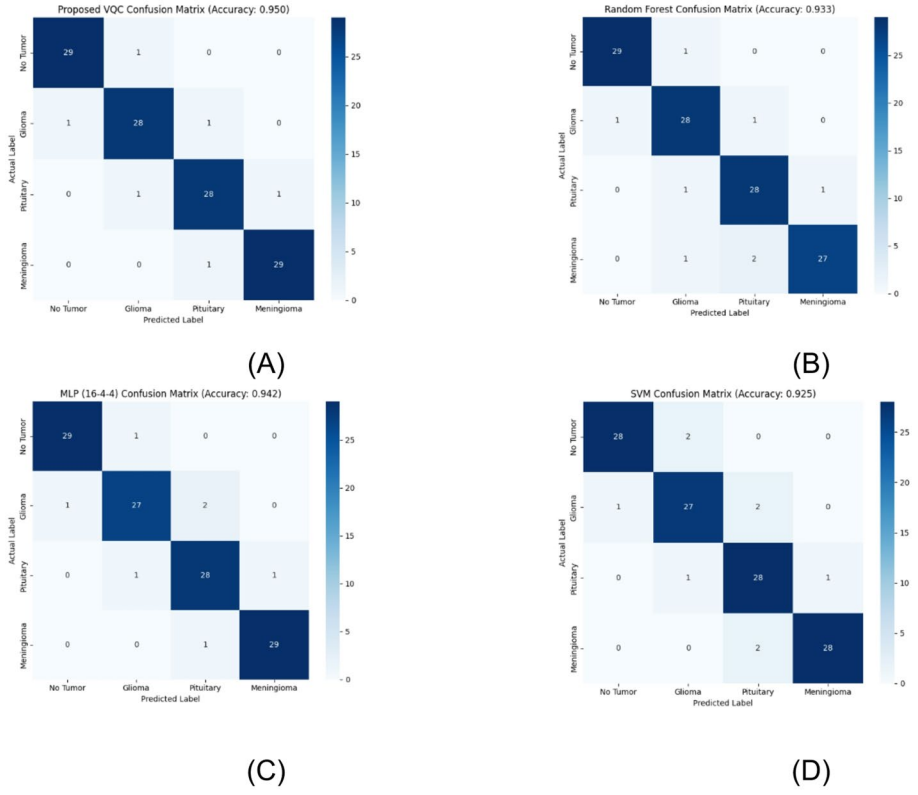

Fig. 8 Confusion Matrix of the Models. **A** VQC Confusion Matrix, **B** Random Forest Confusion Matrix, **C** MLP Confusion Matrix, **D** SVM Confusion Matrix

The test set is used to evaluate the trained model's performance with accuracy score and a detailed classification report, including precision, recall, and F1-score, Specificity and Cohen's Kappa are obtained [35, 36], and given in Table 4.

In addition, the metrics relevant to Quantum approach with a focus on Amplitude Encoding is also evaluated and the outcomes are shown in Table 3.

The confusion matrix of the models are shown in the Fig. 8.

The VQC registered the highest Accuracy 95%, surpassing the competitive performance of other classical models. This performance shown in Figs. 8 and 9, validates the effective feature compression provided by amplitude encoding, which successfully mapped the 16 classical features into the quantum state, allowing the VQC's shallow circuit to capture non-linear decision boundaries more effectively than the tested classical architectures.

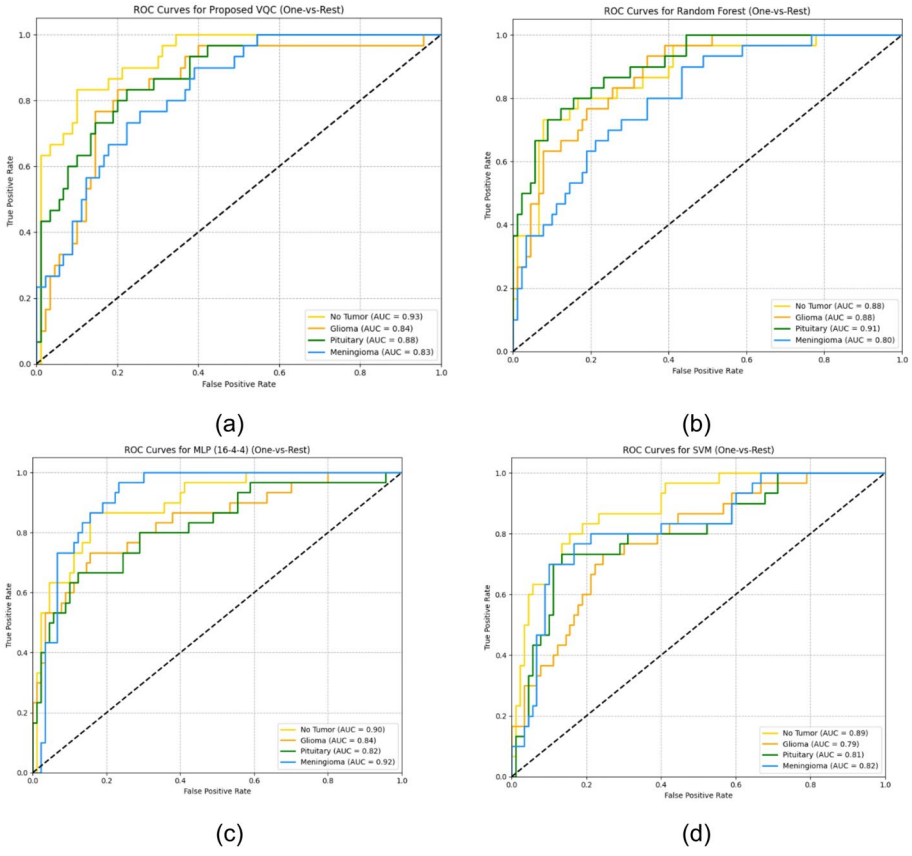

Fig. 9 ROC Curves of the Models. **a** VQC, **b** Random Forest, **c** MLP, **d** SVM

6 Conclusion

This study successfully confirmed the viability and quantitative advantages of using a hybrid quantum-classical approach for brain tumor classification. The key to this superior performance was the strategic application of amplitude encoding after PCA dimensionality reduction. This encoding method was crucial because it exploited the exponential capacity of the quantum state. This allowed the compression of 16 classical features into the minimal 4-qubit Variational Quantum Circuit (VQC)—a feat impossible using linear classical techniques. This unprecedented data loading efficiency enabled the VQC to achieve the highest Accuracy (95%) and superior Specificity (0.983) when compared directly to classical baselines (MLP, RF, and SVM). Furthermore, the VQC's efficiency is remarkable, using only 24 trainable parameters, a 3.5-fold reduction compared to the optimal classical MLP. Furthermore, the reliable convergence, confirmed by a stable 0.11Gradient Norm, validated that the low-depth ansatz successfully avoided the Barren Plateau. These findings confirm that amplitude encoding provides a powerful, NISQ-compatible mechanism to drastically reduce computational complexity, positioning Quantum Machine Learning as a robust and efficient solution for high-dimensional medical image analysis that surpasses classical models. Our future efforts will involve validating this performance on larger quantum systems and testing new encoding strategies.

Author contributions

K. P. Maheswari: Conceptualization, Methodology, Software, Validation, Writing – original draft. Kalaiselvi Thiruvenkadam: Methodology, Writing – review & editing, Conceptualization and Supervision. Sriramakrishnan Pathmanaban: Writing – review & editing, Validation.

Funding
Not applicable.

Data availability
- The datasets used and/or generated during the current study are publicly available in the Brain Tumor MRI Dataset (BraTS) repository in Kaggle. https://www.kaggle.com/datasets/masoudnickparvar/brain-tumor-mri-dataset .- All data necessary for reproducing or verifying the results are included in this published article.- Supplementary data supporting these findings can be obtained from the authors upon a reasonable request.

Declarations

Ethics approval and consent to participate
Not applicable. No human participants were involved in the study.

Consent for publication
Not Applicable. No identifiable images/data of the participants are provided in the manuscript.

Competing interests
The authors declare no competing interests.

Received: 5 August 2025 / Revised: 26 December 2025 / Accepted: 7 January 2026
Published online: 03 March 2026

References

1. Sadoon TA, Ali MHA. Deep learning model for glioma, meningioma and pituitary classification. Int J Adv Appl Sci. 2021;10(1):88–98. https://doi.org/10.11591/ijaas.v10.i1.pp88-98.
2. Yan Q, Liu S, Xu S, Dong C. 3D medical image segmentation using parallel Transformers. Pattern Recogn. 2023;138:109432. https://doi.org/10.1016/j.patcog.2023.109432.
3. Le P, Dong F, Hirota K. A flexible representation of quantum images for polynomial Preparation, image Compression, and processing operations. Quantum Inf Process. 2011;10:63–84.
4. Venegas-andraca SE. S. <>Bose 2003 Storing, processing and retrieving an image using quantum mechanics. Proc SPIE Conf Quantum Inf Comput 5105 137–47.
5. Zhang Y, Lu K, Gao Y, Wang M. NEQR: A novel enhanced quantum representation of digital images. Quantum Inf Process. 2013;12:2833–60.
6. Yan F, Iliyasu AM, Venegas-andraca SE. A survey of quantum image representations. Quantum Inf Process. 2016;15:1–35.
7. Schuld M, Sinayskiy I. F. Petruccione An introduction to quantum machine learning, sep 2014, https://doi.org/10.1080/00107514.2014.964942
8. Biamonte J, Wittek P, Pancotti N, Rebentrost P, Wiebe N, Lloyd S. Quantum Machine Learning,Nature, Volume: 549 - Pages: 195–202, May 2018. https://doi.org/10.1038/nature23474
9. Kosuke Mitarai M, Negoro M, Kitagawa K, Fujii QC, Learning V. 98, Issue: 3–032309, 2018, https://doi.org/10.1103/PhysRevA.98.032309
10. Lloyd S, Mohseni M, Rebentrost P. Quantum algorithms for supervised and unsupervised machine learning, 2013.
11. Mari A, Bromley TR, Izaac J, Schuld M, Killoran N. Transfer learning in quantum neural networks, Volume: 4- 340, 2020. https://doi.org/10.22331/q-2020-10-05-340
12. Afshar PK, Mohammadi A, Plataniotis KN. Brain Tumor Segmentation via Capsule Networks, International Conference on Medical Image Computing and Computer-Assisted Intervention (MICCAI), Lecture Notes in Computer Science, vol 11765.
13. Zhao Y, Yue K, Zhang W, Zhao L, Kuang Z, Access IEEE. 9-79946-79956, 2021, DOI: https://doi.org/10.1109/ACCESS.2021.3084578
14. Joseph. Quantum Machine Learning for Medical Image Analysis: A Review, 2022.
15. Innan N, Bennai M. Simulation of a variational quantum perceptron using grover's algorithm. ArXiv Preprint. 2023. arXiv:2305.11040.
16. Innan N, Khan MAZ, Bennai M. Enhancing quantum support vector machines through variational kernel training. Quantum Inf Process. 2023;22(374). https://doi.org/10.1007/s11128-023-04138-3.
17. Dong Y, Fu Y, Liu H, Che X, Sun L, Luo Y. An improved hybrid quantum-classical convolutional neural network for multiclass brain tumor MRI classification. J Appl Phys. 2023;133(6). https://doi.org/10.1063/5.0138021.
18. Amin J, Anjum MA, Sharif M, Jabeen S, Kadry S, Ger M, P. A new model for brain tumor detection using ensemble transfer learning and quantum variational classifier. Comput Intell Neurosci. 2022. https://doi.org/10.1155/2022/3236305.
19. Bergholm V, arXiv et al. https://arxiv.org/abs/1811, 2018.
20. Khatun A, Aydeniz KY, Weinstein YS, Usman M. Quantum generative learning for high-resolution medical image generation. Mach Learning: Sci Technol. 2025;6(2):025032. https://doi.org/10.1088/2632-2153/add1a9.
21. Ding YF, et al. Adv Eng Inform. 2025;68:103622.
22. Pei JJ, et al. One-to-many image generation model based on parameterized quantum circuits. Digit Signal Proc. 2025;165:105340. https://doi.org/10.1016/j.dsp.2025.105340.
23. Huang SY, An WJ, Zhang DS, Zhou NR. Image classification and adversarial robustness analysis based on hybrid quantum–classical convolutional neural network. Opt Commun. 2023;533:129287. https://doi.org/10.1016/j.optcom.2023.129287.
24. Bravyi S, Gosset D, K¨onig R. Quantum advantage with shallow circuits. Science. 2018;362(6412):308–11.
25. Amin J, Anjum MA, Gul N, Sharif M. A secure two-qubit quantum model for segmentation and classification of brain tumor using MRI images based on blockchain. Neural Comput Appl. 2022;34(20). https://doi.org/10.1007/s00521-022-07388-x.

26. Chandra S, Saxena S, Kumar S, Chaube MK, Bodhey NK, A Novel Framework For Brain Disease Classification Using Quantum Convolutional Neural Network. 2022 IEEE International Women in Engineering (WIE) Conference on Electrical and, Engineering C. (WIECON-ECE). https://doi.org/10.1109/WIECON-ECE57977, 2022.
27. Choudhuri R, Halder A. Brain MRI tumor classification using quantum classical convolutional neural net architecture. Neural Comput Appl. 2023;35(6):4467–78.
28. Parmar SJ, Parmar VR, Verma J, Roy S, Bhattacharya P. Quantum computing: exploring superposition and entanglement for cutting–edge applications, 16th International Conference on Security Information Network (SIN), 2023.
29. Meyer N. A Survey on Quantum Reinforcement Learning, 2022.
30. Chen SY-C. Variational Quantum Circuits for Deep Reinforcement Learning, 2020.
31. Owen Lockwood. Reinforcement Learning with Quantum Variational Circuits, 2020.
32. Andrea Skolik. Quantum agents in the Gym: a variational quantum algorithm for deep Q-learning, 2022.
33. Jules Tillya. The Variational Quantum Eigensolver: a review of methods and best practices, 2022.
34. Brain Tumor MRI, Dataset BTS. https://www.kaggle.com/datasets/masoudnickparvar/brain-tumor-mri-dataset
35. Shajahan S, Pathmanaban S, Tiruvenkadam K. (2024). RIBM3DU-Net: glioma tumour substructures segmentation in magnetic resonance images using residual-inception block with modified 3D U-Net architecture. Int J Imaging Syst Technol, 34(2), e23056.
36. Syedsafi S, Sriramakrishnan P, Kalaiselvi T. (2023, June). An automated two-stage brain tumour diagnosis system using SVM and geodesic distance-based colour segmentation. In International Conference on Power Engineering and Intelligent Systems (PEIS) (pp. 179–191). Singapore: Springer Nature Singapore.

Publisher's Note